

CHARACTERIZATION OF SYNTHETIC APERTURE RADAR IMAGE FEATURES OF THE OCEAN AS A FUNCTION OF WIND SPEED AND HIGH FREQUENCY RADAR PRODUCTS

Ricardo Vicente⁽¹⁾, Jeffrey Paduan⁽²⁾, Benjamin Holt⁽³⁾, Michael Cook⁽²⁾

⁽¹⁾ Instituto Hidrográfico, Rua das Trinas 49 1249-093 Lisboa, Portugal, pires.vicente@marinha.pt

⁽²⁾ Naval Postgraduate School, 699 Dyer Road, Halligan Hall 220A Monterey, CA 93943, USA, paduan@nps.edu, cook@nps.edu

⁽³⁾ Jet Propulsion Laboratory, 4800 Oak Grove Drive Pasadena CA 91109, USA, benjamin.m.holt@jpl.nasa.gov

ABSTRACT

The potential for better understanding of ocean conditions through remote sensing was recognized here with the focus on Synthetic Aperture Radar (SAR) and High Frequency (HF) radar.

The hypothesis that combining remote sensing products may improve results was tested using SAR imagery and available HF radar-derived surface current maps along central California. One SAR image was selected for assessment by evidencing higher correlation in surface current as perceived by both remote sensors.

As expected, wind strength played a dominant role in determining the physical processes visible in the SAR imagery. Moderate wind speed of 2–4 m/s exhibited the most obvious ocean-related processes and the best correlation with features in the HF surface current maps.

Surprising is the discovery that oceanographic features in the SAR imagery represent recent history of tracer advection over hours to days. Thus features in the HF radar daily-average currents appear more highly correlated with features in SAR imagery under moderate wind conditions than the HF radar hourly surface-current snapshots.

1. INTRODUCTION

Knowledge of the oceans is important for all strands of human life, impacting populations economically, socially, politically and strategically. Civilization does not know the world without water, and man's own survival may depend on an understanding of the global ocean and its processes. Navigation, maritime transportation, energy and resource exploitation, naval military operations, search and rescue, oil spill response, recreational activities, and offshore engineering all depend on some degree of information about the ocean. Recent awareness of climate changes has focused media and popular attention on environmental concerns and triggered the hunt for answers. For the last 150 years, oceanographic data have been collected with a large contribution of *in situ* data, particularly after the 1950s and satellite ocean measurements starting in the 1970s [1].

Nowadays, more and more sophisticated sensors are

available for monitoring and deciphering coastal and oceanic processes as near to real time as possible. Remote sensing methods are critical in these efforts. Ocean remote sensing is defined as the use of electromagnetic radiation to acquire information without physically contacting the target or event under investigation [2]. Along with a wide range of sensors, high frequency (HF) radar and synthetic aperture radar (SAR) are of special interest in this present study.

In North America and, in particular, along the central California coast, there exists a large data set of surface currents derived from HF radar observations that can be overlapped with coverage from modern SARs. The combination of both remote sensors has the potential to lead to a high-resolution map of surface features extending from coastline to approximately 100 km offshore, providing 24-hour coverage in all-weather conditions.

This paper lays on [3] research and aims to qualitatively and quantitatively analyze a scenario where SAR and HF radar-derived surface currents are prone to agree. The selected image was chosen from an ensemble of 31 SAR images representative of weak, moderate, and strong wind conditions from a total of 780 archived SAR images, distributed over the period 2007–2010 when the network of HF radar stations was operating relatively continuously.

The imaging mechanisms at work in SAR imagery that can have a significant expression on HF radar-derived surface-current maps include advection of surfactants, convergence/divergence zones, or cross correlation between SAR backscatter, winds, and surface currents on the scale of the HF radar observations. As described in [4], [5] and [6]:

- Advection of surfactants where accumulation of oil slicks indicate current convergence and a darker SAR surface.
- Convergence/divergence zones associated with the interaction between the direction of the long-wave field and the type of surface current, which can in turn lead to divergence, convergence, or shear.
- Atmospheric instability effects where colder air over warmer water causes an increase in surface wind stress due to convective instabilities, thereby

enhancing the backscatter in the presence of warmer ocean surface. When the temperature gradient is large enough, 2 °C or more, the frontal signatures become more evident.

2. SAR AND HF RADAR CHARACTERISTICS

Although both SAR and HF respond to Bragg scattering, they work with distinct frequency bands, detecting different scales of resonant surface waves and, thus, not perceiving the ocean in the same manner. C-band ASAR at 5.3 GHz monitors wind-driven surface roughness caused by capillary waves on the order of 5.6 cm wavelength, with a nominal spatial resolution of 30 m [7], sensing the skin of the ocean, while HF radar, taking as example a frequency of 12 MHz reflects a short gravity wave field with 12 m wavelength to obtain information about radial currents over an area of 3 km and a penetration depth influence close to 1 m.

Having a reasonable assessment of the overlap between SAR and HF radar products requires understanding the differences between these instruments. For this matter, radiation frequency, antenna footprint, and scattering geometry [8] assume particular interest, therefore any method to compare both remote sensor products must be cautiously formulated.

Differences in frequency, and the corresponding Bragg waves' sensitivity that these systems respond to, limit the features one can notice simultaneously on SAR images and HF surface-current maps to eddies, fronts, and convergence/divergence zones. Wind speed, the detection of multiple types of surface features, and frequency place boundaries on the quality and level of detail seen in SAR imagery. Tab. 1 summarizes the most relevant characteristics and specifications of both sensors.

3. DATA

Ocean data have been collected along the central California coast, from Point Reyes to Point Sur, including the areas around San Francisco and Monterey Bay. These data span the period 2007–2010, and they include HF-derived surface current maps, ENVISAT Advanced SAR (ASAR) imagery and *in situ* wind speed and direction. The area is part of the California Current System along the eastern boundary of the north Pacific subtropical gyre [1] which, along with the geomorphology of the coast and bottom topography leads to a wide range of ocean phenomena.

3.1. SAR data

Level 1b SAR imagery presented in this study was processed with NEST (Next ESA SAR Toolbox), using its calibration and georeferencing algorithms, with a nominal resolution of 25 x 25 m for Image Mode Single-Look Complex image (IMS) and 16 x 9 m for

Image Mode Precision image (IMP) products.

Table 1 - Characteristics and specifications of ESA's ENVISAT ASAR C-band and HF CODAR installed in Central California [9], [10], ESA portal (<http://www.esa.int>)

PARAMETER	ENVISAT ASAR	HF RADAR
Country	Europe	USA
Operation	2002–2012	Since 2006
Frequency	5.3 GHz	4- 27 MHz
Bragg wavelength	5.6 cm	5.5 to 35 m
Spatial Resolution Range x Azimuth	IM ~ 30m x 30m	Range: ~3 km Azimuthal: ~5°
Radiometric resolution in range	1.5 - 3.5 dB	N.A.
Radiometric accuracy	0.65 dB	N.A.
No. of looks	IMS = 1, IMP > 3	N.A.
Swath width	IM < 100km	N.A.
Range	Variable w/ mode	30 - 150km
Mean altitude	800 km	Variable w/ terrain
Orbit velocity	7.45 km/s	N.A.
Incident angle	15° - 45° (IS2: 19.2°- 26.7°)	90°
Inclination	98.55°, sun-synchronous	N.A.
Polarization	VV	VV Ground-wave
Measurement cycle	N.A.	20 min
Repeat cycle	35 day	N.A.
Measurement depth	Order of millimeters	< 1m
Accuracy radial current	~ 1 cm/s	~ 10 cm/s

* IM – Image mode, IS2 – Image Swath 2.

** VV – Vertical transmit and vertical receive polarization.

3.2. HF data

HF radar stations collect Bragg backscatter from surface gravity waves, for different depth influences, in accordance with each unit frequency. The Multiple Signal Classification (MUSIC; [11] and [12]) direction-finding algorithm is applied to generate hourly radial currents. Overlapping radials from two or more units are then attached to a pre-defined spatial grid and combined to produce total surface current vectors.

3.3. Surface wind data

Surface wind data is attained from eight buoys, five from the National Data Buoy Center (NDBC), and three from the Monterey Bay Aquarium Research Institute (MBARI), plus five shore stations along Monterey Bay coastal area, provided by the Meteorology Department at Naval Postgraduate School (NPS). The extraction of measured wind speeds and directions is near-concurrent to SAR imagery and the HF radar products' period of observation. All wind vector components are averaged

hourly.

The purpose of retrieving wind measurements over the region of interest is: 1) to evaluate the wind speed during the initial selection process of SAR images from ESA's catalog, in order to have quantitative representation of different wind scales; 2) to assess and interpret ocean SAR features given their dependency on wind-induced surface roughness and to avoid ocean cluttered images [5].

4. SAR FEATURES SEEN IN HF-RADAR SURFACE CURRENT

SAR imagery contains overlapping information of the near-concurrent HF-derived surface currents represented by red vectors as well as *in situ* wind measurements represented by green vectors.

From the SAR image in Figs. 1 and 2, two cases that provide examples of oceanic surface features within the HF-radar large scales are extracted. The image was sensed on 25 May 2008 at 0555 UTC. The local wind is weak ($\sim 3\text{m/s}$) and from the southeast.

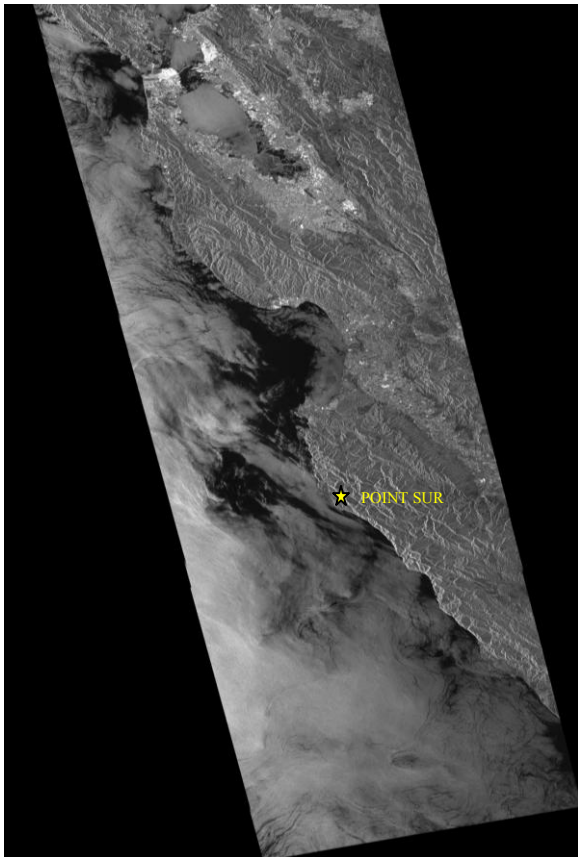


Figure 1. SAR image sensed on 25 May 2008 at 0555 UTC (SAR data provided by ESA).

4.1. Convergence front

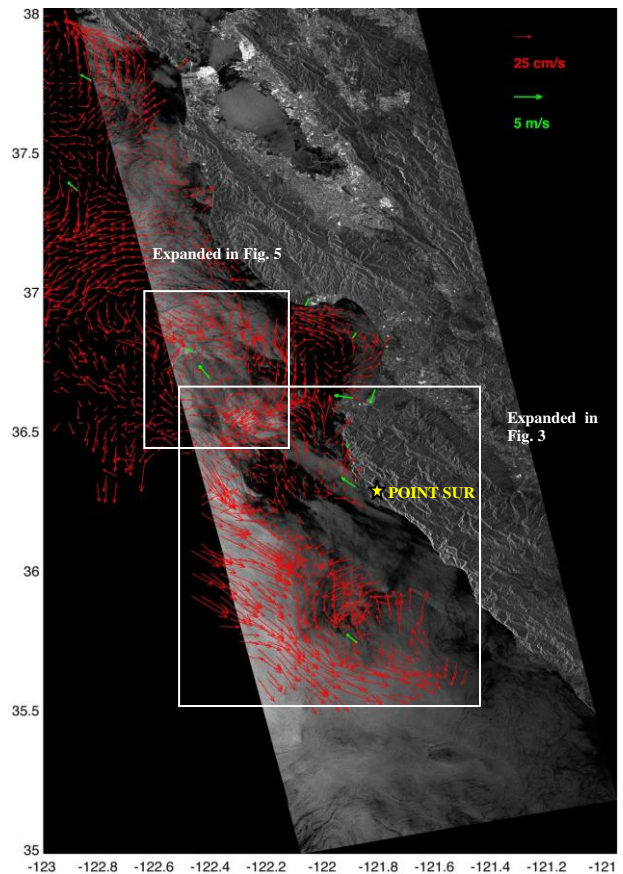


Figure 2. SAR image sensed on 25 May 2008 at 0555 UTC. HF radar currents (red) and surface winds (green) from the closest hour. Both SAR- and HF-radar products detect a frontal signature offshore of Point Sur (details in Fig. 3) and an anti-cyclonic eddy offshore of Monterey (details in Fig. 5). The average wind speed is $\sim 3\text{m/s}$ from southeast (SAR data provided by ESA).

Offshore of Point Sur, Fig. 3 shows a frontal signature seen in SAR with a brighter edge where one of the mechanisms at work is convergence. The visible flow field sensed by the HF-radar indicates the presence of a strong southeastward surface current that turns south and then east, in total agreement with the plume edge. The water mass closer to shore evidences the presence of biogenic slicks which might indicate recent upwelled water. Sea surface temperature map was not available for this period.

Given that, we propose that HF radar and SAR are capable of measuring the same ocean phenomenon under low wind conditions and strong surface currents, providing the features are large enough. The divergence map in Fig. 4 illustrates converging HF-radar currents (inside the black circle) in the Point Sur area, which is coincident with the brighter frontal signature seen in the SAR image in Fig. 3.

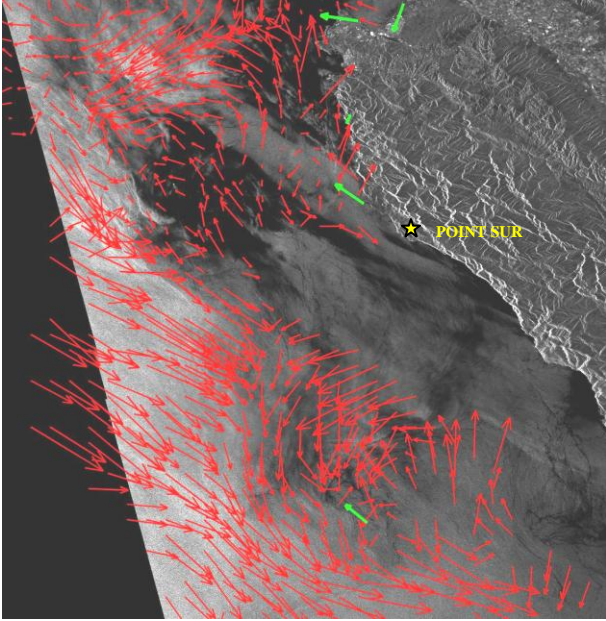


Figure 3. Detail of the SAR image sensed on 25 May 2008 at 0555 UTC, HF radar currents (red) and surface winds (green) from the closest hour. A frontal signature offshore of Point Sur is depicted by both SAR- and HF-radar products (SAR data provided by ESA).

The goal of the horizontal divergence test is to verify, on the scales of HF radar observations, the existence of positive divergence or negative divergence (convergence) compression zones in HF radar surface currents maps.

The horizontal divergence, introduced in [13], derives from the continuity equation, Eq. 1:

$$\frac{du}{dx} + \frac{dv}{dy} = -\frac{dw}{dz} \quad (1)$$

It is inferred, that horizontal divergence implies replacement of water through upwelling, whereas negative horizontal divergence relates to downwelling.

This test computes the spatial derivative of the velocity fields averaged over one hour and linearly fits the results over an area of 10km radius. The result of the test is a scalar with frequency units and it is expected to be bounded by f and $-f$, where $f = 10^{-4} \text{ s}^{-1}$ is the coriolis parameter. The weaker (closer to zero) horizontal divergence values represent small scale phenomena difficult to represent and are removed due to their proximity to the noise levels.

4.2. Vortical feature

The second case, in Fig. 5, shows a detail of an anti-cyclonic eddy offshore of Monterey Bay. The HF-radar surface currents clearly demonstrate a clockwise vortical feature, and the SAR image illustrates a slightly darker core with brighter boundaries and the presence of

slicks. With relatively low wind speed, $\sim 3\text{m/s}$ in this case, the surface current enhancement role is captured on the SAR image.

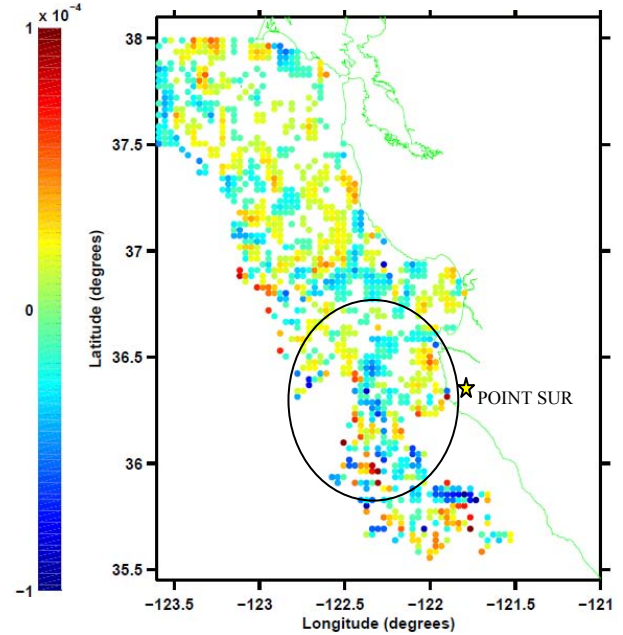


Figure 4. Divergence test shows a convergence feature (bluish dots inside the black circle) centered at 36.4N 122.25W, where the corresponding SAR image demonstrates a brighter frontal structure (Fig. 3).

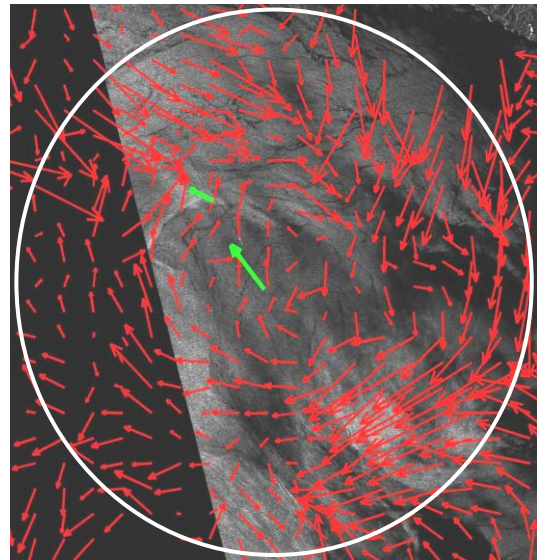


Figure 5. Detail of the SAR image sensed on 25 May 2008 at 0555 UTC, HF radar currents (red) and surface winds (green) from the closest hour. Anti-cyclonic eddy offshore of Monterey Bay is depicted by both SAR- and hourly-averaged HF-radar product (SAR data by ESA).

5. DISCUSSION

A principal hypothesis of the present investigation is to assess the existence of ocean features in the SAR imagery that are correlated to the surface currents as

perceived by HF radar. Some results show ocean features retrieved by HF radar and imaged by SAR, provided the local wind has low intensity, the current field is strong, and the features are large enough. However, a consistent pattern has not been established for the ensemble in [3]. The divergence validation test is positive and encouraging, yet a general conclusion could not be made for the entire ensemble in [3].

There are several possible reasons contributing to a scarcely direct correlation between HF radar-derived surface currents and SAR ocean features, including:

- Surface currents changes to the surface roughness maybe overwhelmed by wind stress contributions. Surface wind is 10 to 20 times more intense than current flow.
- Indirect contribution of the surface current sensed by HF radar via short gravity waves ($\lambda \sim 12m$) compared with the direct effect of wind on the capillary waves sensed by SAR ($\lambda = 5.6cm$ for C-band).
- Poor alignment of the time scales. Although SAR captures the surface image in a 15-second snapshot, it mirrors the resulting distortions preceding atmospheric and oceanic processes of hours-to-days. HF radar maps, on the other hand, represent an hourly-average product of the surface currents, which becomes more instantaneous than the SAR image.

One possibility to bridge the temporal differences between instantaneous HF-radar currents and SAR images is to use HF-radar, daily-average, surface-current map in which tidal and sea breeze effects are naturally removed, instead of the hourly-average product.

Wind speeds below 2-3 m/s cause SAR ocean features to fade and merge with noise levels, though the appropriate enhancement of surface roughness by other imaging processes can lead to the improved sensing of oceanic features. This study revealed that surface winds of 2-4 m/s constitute the suitable level of wind speed required to make assessments of oceanic surface currents influence on C-band SAR images. Hence, future studies in this area should consider assessing SAR data in seasons and time of day when wind speeds are moderate. Strong wind speeds of 10-12 m/s may cause wind clutter to mask most of the ocean surface features and, in cases of large fetch, it may lead to a well-organized atmospheric imprints on the surface layer.

6. REFERENCES

1. Talley L.D., Pickard G.L., Emery W.J., Swift J.H. (2011). *Descriptive Physical Oceanography: An Introduction* (Sixth Edition), Elsevier, Boston
2. Martin, S. (2004), *An Introduction to Ocean Remote Sensing*, Cambridge University press, United Kingdom
3. Vicente, R. (2012). *Characterization of SAR image features of the ocean as a function of wind speed and HF radar products*, (M.S. thesis), Naval Postgraduate School, Monterey, California. Retrieved from: <http://hdl.handle.net/10945/7424> (accessed August, 2013)
4. Clemente-Colon, P., & Xiao-Hai Yan. (1999). Observations of east coast upwelling conditions in synthetic aperture radar imagery. *Geoscience and Remote Sensing, IEEE Transactions on*, 37(5), 2239-2248
5. Holt, B. (2004). SAR Imaging of ocean surface in *Synthetic Aperture Radar Marine User's Manual*. Jackson, C. R & Apel, J. R., eds, NOAA, NESDIS, Office of Research and Applications, Washington, DC. Online at: <http://www.sarusersmanual.com/> (accessed March, 2012)
6. Lyzenga, D. R., Marmorino & G. O., Johannessen, J. A., (2004). Ocean currents and current gradients in *Synthetic Aperture Radar Marine User's Manual*. Jackson, C. R & Apel, J. R., eds, NOAA, NESDIS, Office of Research and Applications, Washington, DC. Online at: <http://www.sarusersmanual.com/> (accessed March, 2012)
7. *ASAR Users Guide*. (n.d.). Retrieved from: <http://envisat.esa.int/handbooks/> (accessed March, 2012)
8. Danilo, C., Chapron, B., Mouche, A., Garello, R. & Collard, F. (2007). Comparisons between HF radar and SAR current measurements in the Iroise sea. *OCEANS 2007 - Europe*, pp. 1-5
9. Graber, H. C., Thompson, D. R. & Carande R. E. (1996). Ocean surface features and currents measured with synthetic aperture radar interferometry and HF radar, *J. Geophys. Res.*, 101(C11), 25813-25832
10. McCandless, A.W. & Jackson C. R. (2004). Principles of synthetic aperture radar in *Synthetic Aperture Radar Marine User's Manual*. Jackson, C. R & Apel, J. R., eds, NOAA, NESDIS, Office of Research and Applications, Washington, DC. Online at: <http://www.sarusersmanual.com/> (accessed March, 2012)
11. Barrick, D. and B. Lipa, (1997). Evolution of bearing determination in HF current mapping radars. *Oceanography*, 10, 72-75
12. Paduan, J. D., Washburn, L. (2013). High Frequency radar observations of ocean surface currents. *Annu. Rev. Mar. Sci.* Vol. 5, 115-136. 10.1146/annurev-marine-121211-172315
13. Sanderson, B. G. (1995), Structure of an eddy measured with drifters, *J. Geophys. Res.*, 100(C4), 6761-6776